Supporting Information

Elucidation of a Redox-Mediated Reaction Cycle for Nickel-Catalyzed Cross Coupling

Rui Sun,[a] Yangzhong Qin,[a] Serge Ruccolo,[a] Christoph Schnedermann,[a] Cyrille Costentin,[b] and Daniel G. Nocera*,[a]

[a] Department of Chemistry and Chemical Biology, Harvard University, 12 Oxford Street, Cambridge, Massachusetts 02138, United States

[b] Laboratoire d'Electrochimie Moléculaire, Unité Mixte de Recherche Université – CNRS No. 7591, Bâtiment Lavoisier, Université Paris Diderot, Sorbonne Paris Cité, 15 rue Jean de Baïf, 75205 Paris Cedex 13, France

Email: dnocera@fas.harvard.edu

Table of Contents

A. General Considerations

Commercial reagents were stored in a N_2-filled glovebox and used without further purification. All liquid reagents and deuterated solvents were degassed by three cycles of freeze-pump-thaw and stored over activated 3 Å molecular sieves. 4′-bromoacetophenone, $NiCl_2(dme)$ (dme = 1,2-dimethoxyethane), dtbbpy (dtbbpy = 4,4′-di-tert-butyl-2,2′-dipyridyl), the iridium photocatalyst [Ir(dF-CF$_3$-ppy)$_2$(dtbbpy)][PF$_6$], 1,3-benzodioxole, 2-bromotoluene, 2,4-bis(trifluoromethyl)-bromobenzene and n-Bu$_4$NBF$_4$ were purchased from Sigma-Aldrich. Quinuclidine was purchased from Alfa Aesar. Ni(cod)$_2$ (cod = 1,5-cyclooctadiene) was purchased from STREM. All non-deuterated solvents were purified by the method of Grubbs and stored over activated 3 Å molecular sieves.[1] n-Bu$_4$NBF$_4$ was dried *in vacuo* at 80 °C overnight before use. All manipulations were performed with the rigorous exclusion of air and moisture unless otherwise stated. ^{1}H NMR spectra were recorded at the Harvard University Department of Chemistry and Chemical Biology NMR facility on an Agilent DD2 spectrometer operating at 600 MHz or a Varian Unity/Inova spectrometer operating at 500 MHz. EPR spectra were recorded on a Bruker ElexSys E500 spectrometer. The Ni(II) complexes (dtbbpy)Ni(2,4-bis(CF$_3$)phenyl)(OCH$_2$CF$_3$) and (dtbbpy)Ni(o-tolyl)(Br) were prepared according to reported procedures.[2,3] Solutions of Ni(dtbbpy)(cod) were prepared *in-situ* using an adapted literature procedure by adding CH_3CN to a vial charged with Ni(cod)$_2$ and dtbbpy (1:1 mol ratio) and stirring for 1 h at ambient temperature.[4] Solutions of (dtbbpy)NiCl$_2$ were prepared *in-situ* by adding CH_3CN to a vial charged with $NiCl_2(dme)$ and dtbbpy (1:1 mol ratio), sonicating for 30 min at ambient temperature, and filtering with a 0.22 μm PTFE syringe filter.

B. Quantum Yield Measurements

The reaction mixtures were prepared by adding 5.5 mL of CD_3CN to a 20 mL scintillation vial charged with 4′-bromoacetophenone (273.7 mg, 1.38 mmol), methanol (66.1 mg, 2.06 mmol), quinuclidine (168.2 mg, 1.51 mmol), dtbbpy (18.4 mg, 68.7 μmol), $NiCl_2(dme)$ (15.1 mg, 68.7 μmol), [Ir(dF-CF$_3$-ppy)$_2$(dtbbpy)][PF$_6$] (15.4 mg, 13.7 μmol), and 1,3-benzodioxole in the glovebox. The vial was then sealed with electrical tape and the mixture was sonicated at ambient temperature for 30 min, before being passed through a 0.22 μm PTFE syringe filter. An aliquot of the solution was drawn and transferred into a 1.0 cm quartz cuvette equipped with a magnetic stir bar for each quantum yield measurement. The samples were irradiated using a 150 W Xe arc lamp (Newport 67005 arc lamp housing and 69907 power supply) under fan cooling and vigorous stirring. A 435 nm line filter was employed to generate a monochromatic beam, which was further focused with a focusing lens (f = 4 cm) onto the sample. The photon flux was measured by chemical actinometry against 0.15 M potassium ferrioxalate according to a standard procedure.[5] Measurements of the power-dependence were carried out by placing neutral density filters before the focusing lens to attenuate the photon flux. Product yields were determined by ^{1}H NMR spectroscopy against 1,3-benzodioxole as an internal standard. Each reaction was carried out in triplicate. The quantum yields are shown in Table S1 along with average percent yields obtained under each condition as determined against 1,3-benzodioxole.

Table S1. Quantum yield as a function of power.

Power (mW)	Percent Yield of Product	Quantum Yield[a]
0.08	28%	25 ± 3
0.34	17%	11.5 ± 0.4
1.43	10%	3.5 ± 0.3
3.54	10%	2.6 ± 0.2
7.16	7%	1.9 ± 0.2
10.95	9%	1.63 ± 0.08

[a] quantum yield = mol product/mol photons absorbed

C. Faradaic Yield Measurements

The reaction mixtures were prepared by adding 16 mL of a 0.1 M n-Bu$_4$NBF$_4$ electrolyte solution in CH$_3$CN to a 20 mL scintillation vial charged with 4′-bromoacetophenone (746.6 mg, 3.75 mmol), methanol (180.2 mg, 5.62 mmol), quinuclidine (458.6 mg, 4.12 mmol), dtbbpy (50.3 mg, 188 μmol), and NiCl$_2$(dme) (41.3 mg, 188 μmol). The vial was sealed with electrical tape and sonicated at ambient temperature for 30 minutes before being passed through a 0.22 μm PTFE syringe filter. A 5.0 mL aliquot of the solution was drawn and transferred to a divided H-cell for each measurement. Cathodic galvanostatic electrolysis was performed using a glassy carbon rod working electrode (3.0 mm diameter) wrapped with PTFE tape to expose only ~1 cm of its total length to the solution. A non-aqueous Ag/Ag$^+$ reference electrode and reticulated vitreous carbon counter electrode were used. The same working electrode was used for each reaction and washed with 3×2 mL CH$_3$CN between electrolyses to ensure a consistent surface area. The electrolysis time was adjusted such that 0.90 C of charge was passed in each experiment. The solution was taken from the cathodic compartment at the completion of electrolysis and the solvent removed *in vacuo*. 1.0 mL of a solution containing 1,3-benzodioxole in CD$_3$CN was added to dissolve the residue and product yield was determined by ^{1}H NMR against 1,3-benzodioxole. Each reaction was carried out in triplicate. The faradaic yields are shown in Table S2 along with average percent yields obtained under each condition as determined against 1,3-benzodioxole.

Table S2. Faradaic yield as a function of cathodic current.

Current (mA)	Percent Yield of Product	Faradaic Yield[b]
0.1	14%	19 ± 2
0.25	10%	13.6 ± 0.3
0.5	6%	7.6 ± 1.0
0.75	5%	7.2 ± 0.6
1	4%	5.6 ± 0.8

[b] faradaic yield = mol product/mol electrons absorbed

D. Control Experiments

Catalytic activity without photo- or electrochemical activation. 2.0 mL of CD$_3$CN were added to an amber vial charged with 4′-bromoacetophenone (99.5 mg, 0.5 mmol), methanol (24.0 mg, 0.75 mmol), dtbbpy (6.7 mg, 0.025 mmol), NiCl$_2$(dme) (5.5 mg, 0.025 mmol), quinuclidine (61.1 mg, 0.55 mmol), and 1,3-benzdioxole as an internal standard. The reaction mixture was stirred for 30 min with rigorous exclusion of light and passed through a 0.22 μm PTFE syringe filter. A 1.0 mL aliquot was drawn and added to an amber vial charged with [Ir(dF-CF$_3$-ppy)$_2$(dtbbpy)][PF$_6$] (2.8 mg, 2.5 μmol). Both the solution containing the Ir photocatalyst and the remainder of that without were transferred to two separate J. Young NMR tubes wrapped with aluminum foil. ^{1}H NMR spectra taken after three days showed no product formation from either sample.

Photochemical activity in the absence of the Ir photocatalyst. 2.0 mL of CD$_3$CN were added to an amber vial charged with 4′-bromoacetophenone (99.5 mg, 0.5 mmol), methanol (24.0 mg, 0.75 mmol), dtbbpy (6.7 mg, 0.025 mmol), NiCl$_2$(dme) (5.5 mg, 0.025 mmol), quinuclidine (61.1 mg, 0.55 mmol), and 1,3-benzdioxole as an internal standard. The reaction mixture was stirred for 30 min with rigorous exclusion of light and passed through a 0.22 μm PTFE syringe filter. A 1.0 mL aliquot was drawn, transferred to a J. Young NMR tube, and placed before a blue LED light source with fan cooling. The product yield was measured to be 48% by ^{1}H NMR against 1,3-benzodioxole after 24h of irradiation.

Photochemical activity in the absence of quinuclidine. 3.0 mL of CD$_3$CN were added to an amber vial charged with 4'-bromoacetophenone (150 mg, 0.75 mmol), methanol (36 mg, 1.12 mmol), dtbbpy (10 mg, 0.038 mmol), NiCl$_2$(dme) (8.2 mg, 0.038 mmol), and 1,3-benzodioxole as an internal standard. The reaction mixture was stirred for 30 min with rigorous exclusion of light and passed through a 0.22 μm PTFE syringe filter. A 1.0 mL aliquot was drawn and added to a scintillation vial charged with K$_2$CO$_3$ (38 mg, 0.28 mmol) and [Ir(dF-CF$_3$-ppy)$_2$(dtbbpy)][PF$_6$] (2.8 mg, 2.5 μmol). The vial was sealed with electrical tape and placed before a blue LED light source with fan cooling. The product yield was measured to be 37% by ^{1}H NMR against 1,3-benzodioxole after 24 h of irradiation.

Time-dependence of the faradaic yield. To exclude the possibility that the trend observed in Figure 3C is due to changes in electrolysis time, we decided to measure the faradaic yield under cathodic galvanostatic electrolysis at 0.5 mA for different lengths of time. The reaction mixtures were prepared by adding 16 mL of a 0.1 M *n*-Bu$_4$NBF$_4$ electrolyte solution in CH$_3$CN to a 20 mL scintillation vial charged with 4′-bromoacetophenone (746.6 mg, 3.75 mmol), methanol (180.2 mg, 5.62 mmol), quinuclidine (458.6 mg, 4.12 mmol), dtbbpy (50.3 mg, 188 μmol), and NiCl$_2$(dme) (41.3 mg, 188 μmol). The vial was sealed with electrical tape and sonicated at ambient temperature for 30 min before being passed through a 0.22 μm PTFE syringe filter. A 5.0 mL aliquot of the solution was drawn and transferred to a divided H-cell for each measurement. Cathodic galvanostatic electrolysis was performed using a glassy carbon rod working electrode (3.0 mm diameter) wrapped with PTFE tape to expose only ~1 cm of its total length to the solution. A non-aqueous Ag/Ag$^+$ reference electrode and reticulated vitreous carbon counter electrode were used. The same working electrode was used for each reaction and

washed with 3 × 2 mL CH$_3$CN between electrolyses to ensure a consistent surface area. The solution was taken from the cathodic compartment at the completion of electrolysis and the solvent removed *in vacuo*. 1.0 mL of a solution containing 1,3-benzodioxole in CD$_3$CN was added to dissolve the residue and product yield was determined by ^{1}H NMR against 1,3-benzodioxole. The calculated faradaic yield as a function of electrolysis time from 15 min to 90 min was invariant with a value of 8.0 ± 1.4%.

E. Dynamic Stern-Volmer Measurements

The nanosecond time-resolved emission spectroscopy setup was previously described in detail.[6] A Quanta-Ray Nd:YAG laser (SpectraPhysics) provides 3rd harmonic laser pulses at 355 nm with a repetition rate of 10 Hz and pulse width of ~10 ns (FWHM). A further MOPO (SpectraPhysics) was used to provide tunable laser pulses in the visible region. Typical excitation energy was adjusted to ~1 mJ/pulse. The dynamic Stern-Volmer quenching studies were carried out with 20 μM $[Ir(dF\text{-}CF_3\text{-}ppy)_2(dtbbpy)][PF_6]$ in CH_3CN both in the presence and absence of quencher. All samples were prepared in a N_2-filled glovebox and sonicated for 30 min at ambient temperature before being passed through a 0.22 μm PTFE syringe filter. Different samples were obtained by sequentially diluting a stock solution of the quencher and photocatalyst with a solution containing only the photocatalyst. Measurements were taken with vigorous magnetic stirring. The emitted light was collected by a pair of lenses and sent to a spectrometer (Triax 320) where the selected emission wavelength could be detected. Typically, the signal at 500 nm was selected and recorded by a PMT coupled to an oscilloscope (LeCroy 9384CM). The emission decays were fitted with mono-exponential functions and the lifetimes (τ) were extracted accordingly. The results of SV dynamic quenching of the Ir(III) photocatalyst excited state by quinuclidine (— pink) and $(dtbbpy)NiCl_2$ are shown in Figure S1.

Figure S1 | A Dynamic Stern-Volmer quenching plot for the Ir(III) excited state under different concentrations of quinuclidine (— pink) and $(dtbbpy)NiCl_2$ (— bl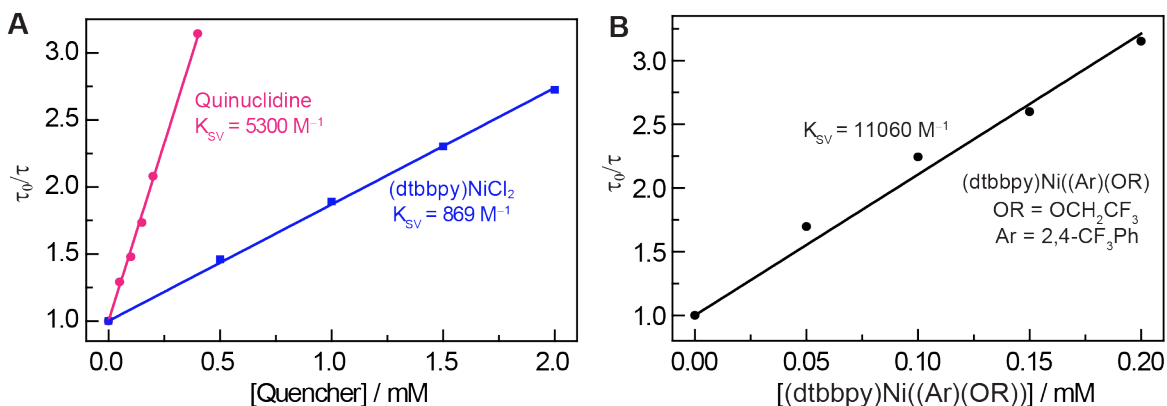ue). **B** Dynamic Stern-Volmer quenching plot for the Ir(III) excited state under different concentrations of $(dtbbpy)Ni(2,4\text{-}bis(CF_3)phenyl)(OCH_2CF_3)$. τ and τ_0 represent the measured fluorophore lifetime in a solution with and without quencher, respectively.

F. Single-Wavelength Kinetic Studies and Transient Absorption Spectroscopy

The nanosecond transient absorption (TA) spectroscopy setup was described previously in detail.[6] All samples were prepared in a N_2-filled glovebox and sonicated for 30 min at ambient temperature before being passed through a 0.22 μm PTFE syringe filter. For single-wavelength kinetic studies, samples containing different concentrations of the additive under study (quinuclidine or (dtbbpy)NiCl$_2$) were obtained by sequential dilution of a concentrated stock solution including all compounds with a solution which excluded the additive. The samples were sparged with N_2 gas in a 40 mL volatile organic analyte sampling vial (Restek) during experiments and flown through a 1.0 cm flow cell (Starna) with a peristaltic pump for spectral acquisition. Single-wavelength kinetic studies for probing the stability of complex **1** are shown in Figure S2. The time-resolved TA spectra for a solution containing [Ir(dF-CF$_3$-ppy)$_2$(dtbbpy)]-[PF$_6$] and quinuclidine in the absence and presence of (dtbbpy)NiCl$_2$ are shown in Figures S3 and S4, respectively.
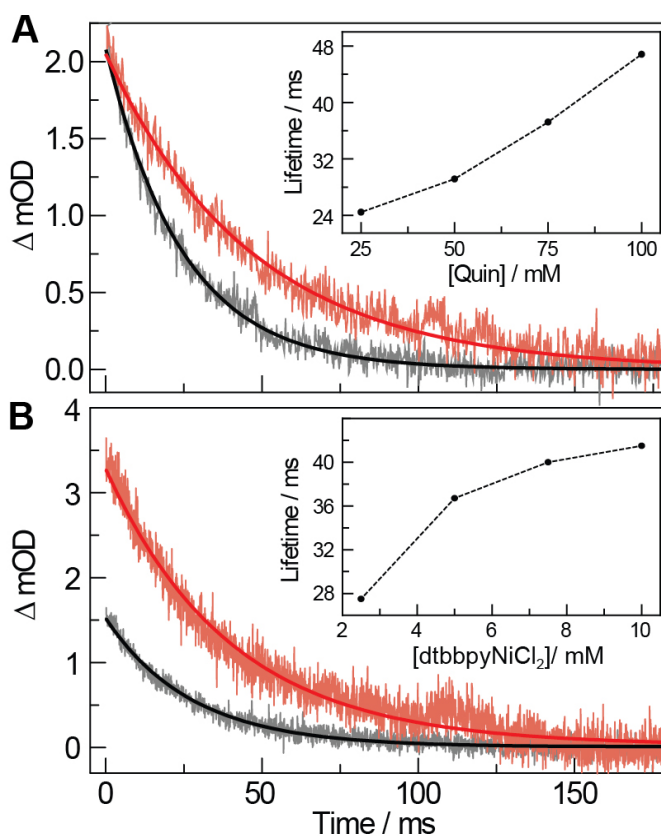
Figure S2 | Single-wavelength kinetic traces (λ_{exc} = 425 nm) monitored at 670 nm. **A** Kinetic trace of a solution containing 0.2 mM [Ir(dF-CF$_3$-ppy)$_2$(dtbbpy)][PF$_6$], 5 mM (dtbbpy)NiCl$_2$, and 100 mM 4'-bromoacetophenone with 25 mM (— grey) and 100 mM (— orange) quinuclidine. **B** Kinetic trace of a solution containing 0.2 mM [Ir(dF-CF$_3$-ppy)$_2$(dtbbpy)][PF$_6$], 100 mM 4'-bromoacetophenone, and 50 mM quinuclidine with 2.5 mM (— grey) and 10 mM (— orange) (dtbbpy)NiCl$_2$. Solid lines show mono-exponential fits and insets show the fitted lifetime in the presence of different concentrations of the additive under study.
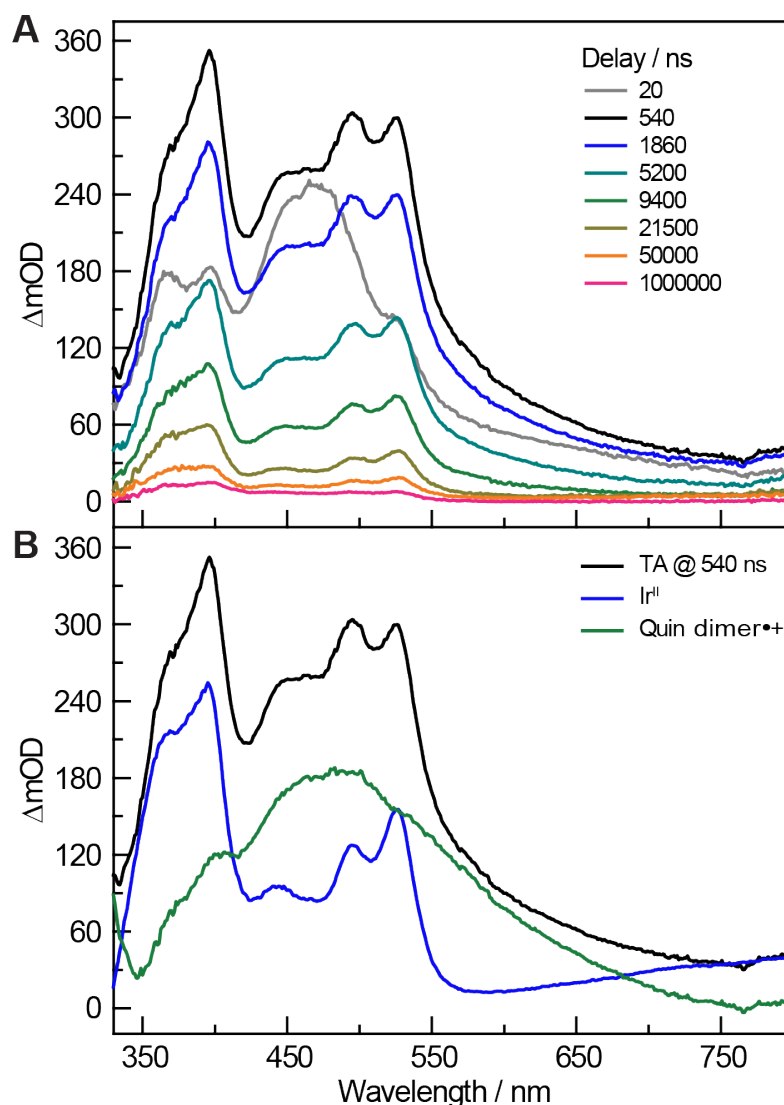
Figure S3 | TA study of the Ir(III) photocatalyst in the presence of quinuclidine. **A** Evolution of the TA spectra after photoexciting (λ_{exc} = 355 nm) a solution of 0.2 mM [Ir(dF-CF$_3$-ppy)$_2$(dtbbpy)][PF$_6$] and 25 mM quinuclidine in CH$_3$CN. **B** Possible deconvolution of the TA spectrum at 540 ns (━ black) when the Ir(III) excited state completely disappears. The spectrum of a transient intermediate (━ green) was obtained by subtracting the Ir(II) contribution (━ blue) obtained by spectroelectrochemistry (see Figure S6) from the TA spectrum at 540 ns with minimization of the first derivative of the resultant spectrum with respect to wavelength. The spectral features of this intermediate are consistent with those of a quinuclidine dimer radical cation (see Figure S14).[7]
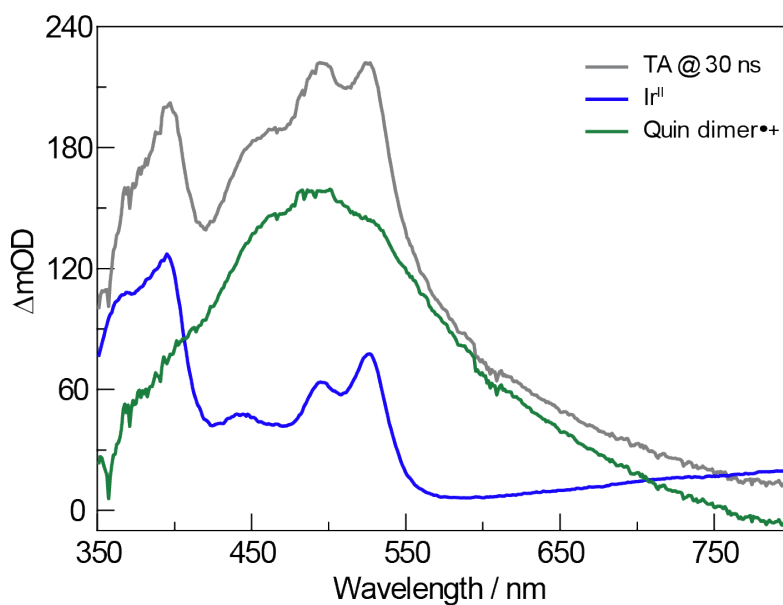
Figure S4 | Deconvolution of the TA spectrum at 30 ns after photoexciting (λ_{exc} = 425 nm) a solution of 0.2 mM [Ir(dF-CF$_3$-ppy)$_2$(dtbbpy)][PF$_6$], 5 mM NiCl$_2$(dme), 5 mM dtbbpy, and 50 mM quinuclidine in CH$_3$CN. The Ir(II) spectrum (━ blue) was obtained by spectroelectrochemistry (see Figure S6). The quinuclidine dimer radical cation spectrum (━ green) was obtained by subtracting the Ir(II) contribution from the TA spectrum at 30 ns with minimization of the first derivative of the resultant spectrum with respect to wavelength. The quinuclidine dimer radical cation spectrum thus obtained is similar to that in Figure S2B, confirming that quinuclidine dominates the quenching of the Ir(III) excited state in the presence of (dtbbpy)NiCl$_2$.

G. Cyclic Voltammetry and Spectroelectrochemistry

All electrochemical experiments were performed with a CH Instruments 760D Electrochemical Workstation (Austin, Texas) and CHI Version 10.03 software in a N_2-filled glovebox. The studied compounds were dissolved in an electrolyte solution containing 0.1 M n-Bu$_4$NBF$_4$ in CH$_3$CN. A three-electrode undivided cell configuration with a Pt wire counter electrode and a non-aqueous Ag/Ag$^+$ reference electrode was used for all cyclic voltammetry (CV) experiments. All working electrodes were sequentially polished on felt using diamond pastes of 3 μm and 1 μm before use. The CV of a 1 mM solution of ferrocene (Fc) was taken at the start of every experiment. Spectroelectrochemical measurements were performed using a 0.5 mm thin-layer quartz cuvette with a Pt mesh working electrode, non-aqueous Ag/Ag$^+$ reference electrode, and Pt wire counter electrode. All samples were first sonicated for 30 minutes at ambient temperature and subsequently passed through a 0.22 μm PTFE syringe filter. The UV-vis absorption spectra were recorded with OceanView 1.4.1 coupled with a light source (Ocean Optics DT-MINI-2GS) and spectrometer (Ocean Optics, USB4000). The CV for [Ir(dF-CF$_3$-ppy)$_2$(dtbbpy)][PF$_6$] and spectroelectrochemistry for the complex's reduction are shown in Figures S5 and S6, respectively.
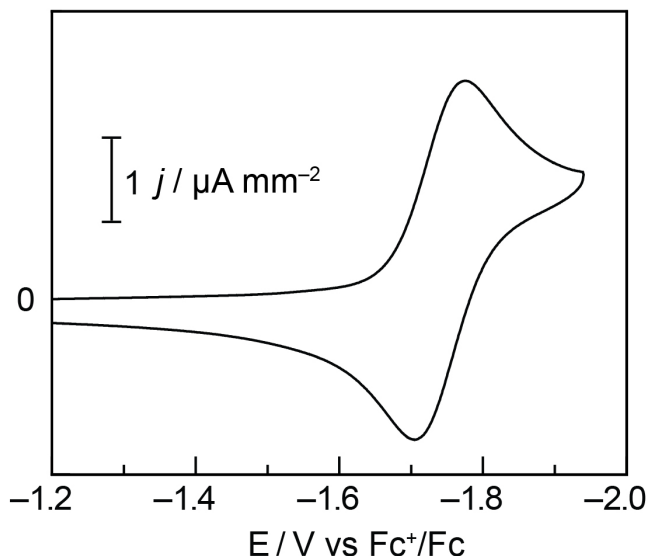
Figure S5 | CV of a 1.0 mM solution in CH$_3$CN of the Ir(III) photocatalyst [Ir(dF-CF$_3$-ppy)$_2$(dtbbpy)][PF$_6$] taken with a 3.0 mm glassy carbon (GC) working electrode at v = 0.1 V s^{-1}. $E_{1/2}$ = −1.74 V.
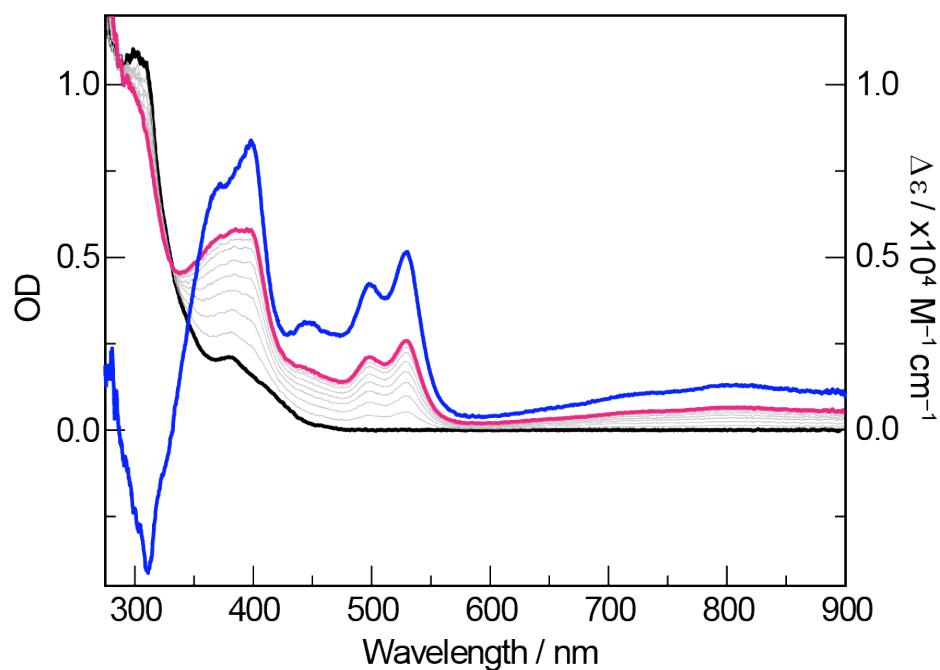
Figure S6 | Spectroelectrochemistry in CH$_3$CN of [Ir(dF-CF$_3$-ppy)$_2$(dtbbpy)][PF$_6$] under a cathodic potential of −1.8 V vs Fc$^+$/Fc showing a transition from the Ir(III) state (▬ black) to an Ir(II) state (▬ pink). The difference in extinction coefficients between the Ir(II) and Ir(III), △ε (▬ blue), is shown against the right axis.
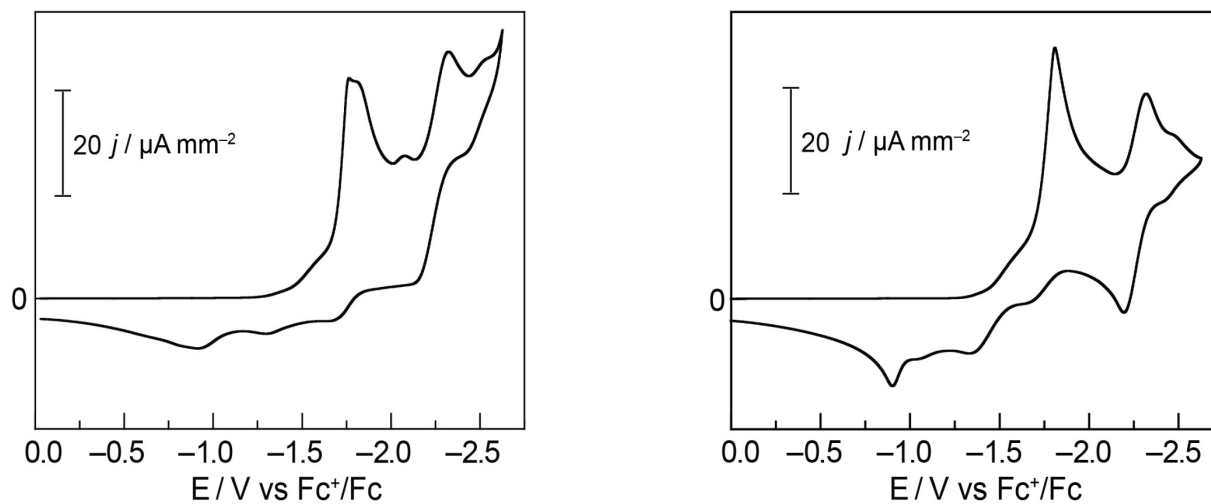
Figure S7 | CV of a CH$_3$CN solution containing 12.5 mM NiCl$_2$(dme), 12.5 mM dtbbpy, 275 mM quinuclidine (left) in the presence of 375 mM methanol (corresponding to initial concentrations in the photoredox reaction) and (right) in the absence of methanol. Thee working electrode was 3.0 mm GC and the scan rate was v = 0.1 V s^{-1}.
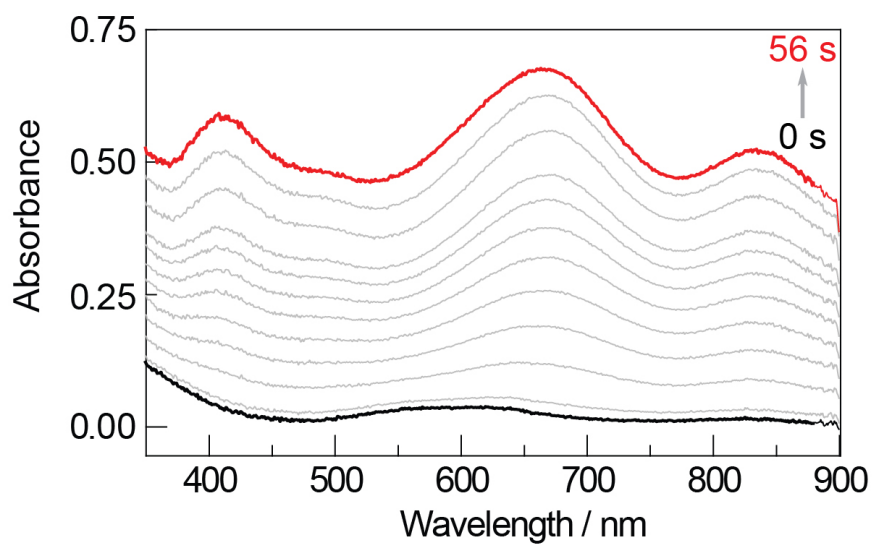
Figure S8 | Spectroelectrochemistry of a CH$_3$CN solution containing 12.5 mM NiCl$_2$(dme), 12.5 mM dtbbpy, and 275 mM quinuclidine under a cathodic potential of −1.74 V showing a transition from the initial Ni(II) state (▬ black) to a state with spectroscopic features consistent with complex **1** (▬ red).

H. *In Situ* Spectroscopic Monitoring of the Photoredox Reaction

We designed the apparatus shown in Figure S9 to probe transient intermediates that accumulate during the photochemical reaction. A focusing lens (f = 4 cm) was placed before a Kessil A160WE Controllable LED Aquarium Light, which was used to excite the sample placed inside the holder coupled to a S.I. Photonics Model 400 Series UV-vis spectrophotometer equipped with a deuterium light source and charge-coupled device (CCD) detector. All spectra were blank-corrected against the appropriate solvent. The sample solutions were prepared by adding 4 mL CH_3CN to a 20 mL scintillation vial charged with 4′-bromoacetophenone (199.0 mg, 1.0 mmol), 1-hexanol (133.2 mg, 1.5 mmol), quinuclidine (122.3 mg, 1.1 mmol), dtbbpy (13.4 mg, 50 μmol), $NiCl_2(dme)$ (11.0 mg, 50 μmol), and $[Ir(dF\text{-}CF_3\text{-}ppy)_2(dtbbpy)][PF_6]$ (11.2 mg, 10 μmol). The vial was then sealed with electrical tape and sonicated for 30 minutes at ambient temperature, before being passed through a 0.22 μm PTFE syringe filter. The solution was then transferred to a 1.0 cm quartz cuvette equipped with a magnetic stir bar for spectroscopic measurements.
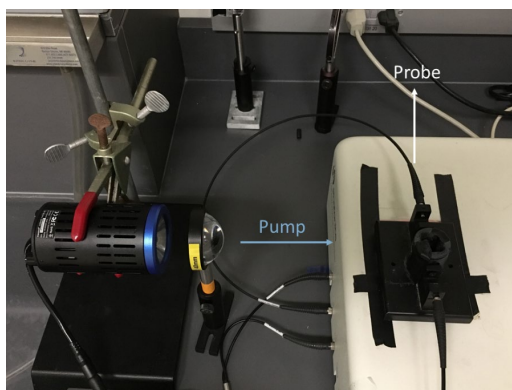
Figure S9 | Apparatus used for *in situ* monitoring of the photochemical reaction.
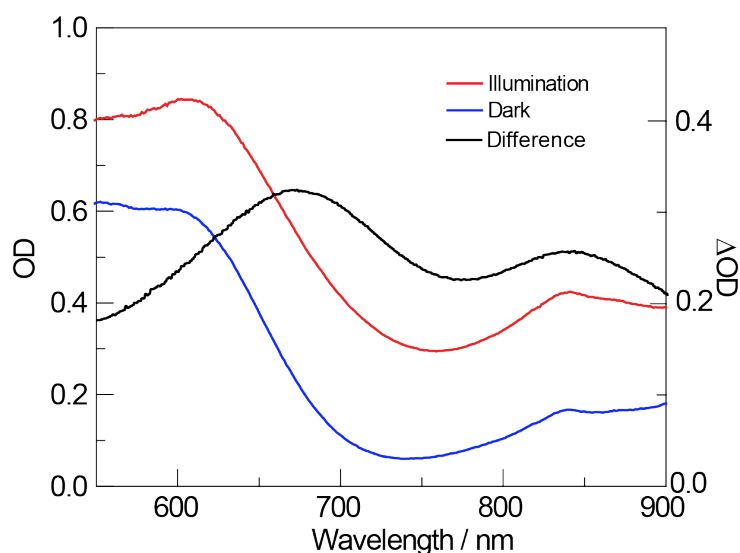
Figure S10 | *In situ* monitoring of the photoredox reaction showing the absorption spectrum of the reaction solution after 1 min of irradiation (━ red) and in the dark (━ blue). The difference spectrum (━ black) was obtained by subtracting the dark spectrum from that while under illumination.

I. Preparation and Characterization of the Paramagnetic Ni Intermediate 1

Comproportionation experiment. Comproportionation studies were carried out in a N_2-filled glovebox by the dropwise addition of 2 mL of a 300 μM CH_3CN solution of Ni(dtbbpy)(cod) to 2mL of one containing 5 mM of (dtbbpy)NiCl$_2$ in the presence and absence of quinuclidine (275 mM). The resulting samples were left to stir for 5 minutes before being passed through a 0.22 μm PTFE syringe filter. Absorption spectra were collected with a 0.5 mm quartz cell using a spectrophotometer equipped with a CCD detector.
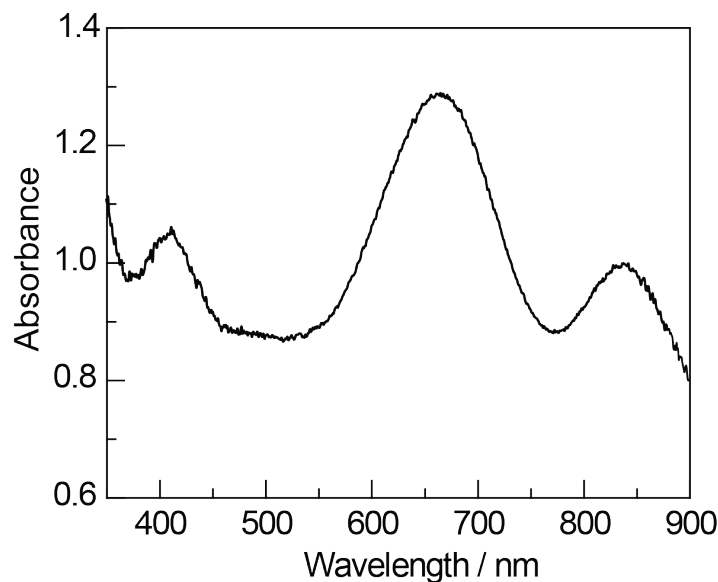
Figure S11 | Spectroscopic study of the comproportionation reaction performed in the presence of quinuclidine. In the absence of quinuclidine, no discernible spectrum is observed.

Stability of 1 towards dilution. A stock solution of **1** was prepared *via* the dropwise addition of 5 mL of a 12.5 mM CH_3CN solution of Ni(dtbbpy)(cod) into 5 mL of a sample containing NiCl$_2$(dme) (13.7 mg, 62.5 μmol), dtbbpy (16.8 mg, 62.7 μmol), and quinuclidine (152.9 mg, 1.38 mmol) that had been sonicated for 30 min at ambient temperature. The resulting dark green solution was left to stir for 30 min before being passed through a 0.22 μm PTFE syringe filter. This solution was then diluted 10× with solutions containing only 275 mM quinuclidine (Figure S12A, blue trace) and 275 mM quinuclidine in the presence of 12.5 mM (dtbbpy)NiCl$_2$ (Figure S12A, red trace). Absorption spectra were taken with a 1.0 cm quartz cuvette on a Varian Cary 5000 UV-vis-NIR spectrophotometer.
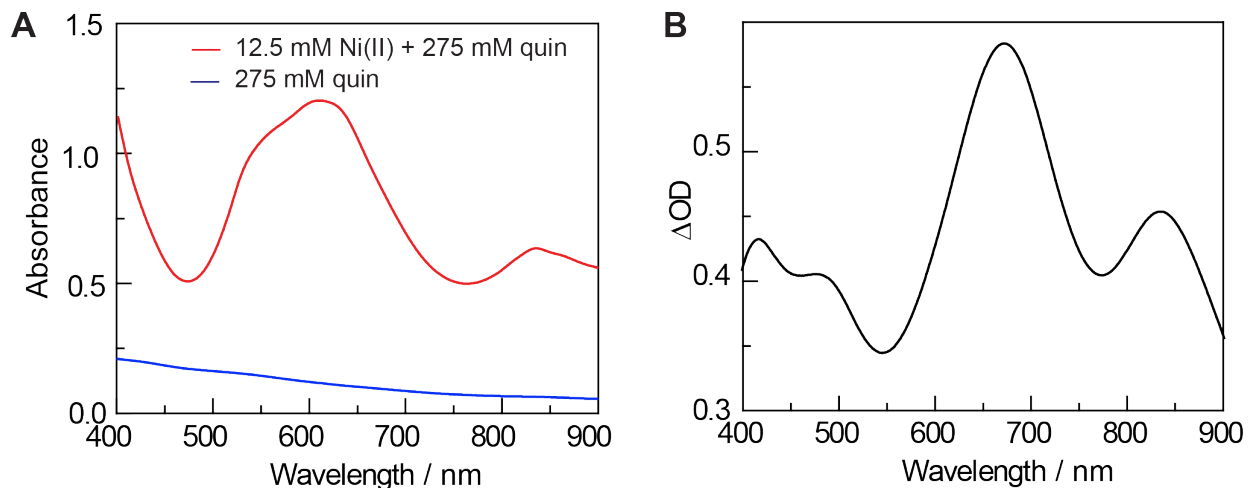
Figure S12 | Stability of **1** towards dilution. **A** Dilution of Ni(I) in the presence of quinuclidine (━ blue) and both (dtbbpy)NiCl₂ and quinuclidine (━ red), demonstrating the decomposition of Ni(I) upon dilution in the absence of excess (dtbbpy)NiCl₂. **B** Difference spectrum of the sample diluted in the presence of (dtbbpy)NiCl₂ and quinuclidine after air exposure shows that the characteristic spectroscopic features of **1** were retained under these conditions.

EPR spectroscopy. 5 mL of a CH_3CN solution containing Ni(dtbbpy)(cod), prepared from Ni(cod)₂ (34.4 mg, 0.125 mmol) and dtbbpy (33.6 mg, 0.125 mmol), were added dropwise in a N₂-filled glovebox to a 5 mL sample containing (dtbbpy)NiCl₂ and quinuclidine, which was prepared by adding CH_3CN to a vial charged with (dme)NiCl₂ (137.3 mg, 0.625 mmol), dtbbpy (167.8 mg, 0.625 mmol), and quinuclidine (160 mg, 1.44 mmol) and sonicating for 30 min at ambient temperature. The dark green solution obtained after addition was left to stir for 30 min, passed through a 0.22 μm PTFE syringe filter, and transferred to an EPR tube. The EPR spectrum was collected on a frozen solution at 77 K.

J. Measurement of the Turnover Number (TON)

Complex 1. 1 mL of a solution in CH_3CN containing 12.5 mM Ni(dtbbpy)(cod) and 275 mM quinuclidine was prepared and added dropwise to 2 mL of a sample containing 18.8 mM (dtbbpy)NiCl$_2$ and 275 mM quinuclidine to give a 8.3 mM solution of **1** assuming a 1:2 stoichiometry for the conversion of Ni(0) into **1**. The dark green solution was stirred for 30 min before being passed through a 0.22 μm PTFE syringe filter. 0.6 mL of this concentrated sample was diluted with 5 mL of a CH_3CN solution containing 18.8 mM (dtbbpy)NiCl$_2$ and 275 mM quinuclidine, corresponding to a 10× dilution. 0.5 mL of the 8.3 mM solution of **1** was added dropwise to 0.5 mL of a stirred solution of substrate in CH_3CN containing 250 mM 4′-bromoacetophenone, 375 mM methanol, 275 mM quinuclidine, and 12.5 mM (dtbbpy)NiCl$_2$. Similarly, 5.0 mL of the 0.83 mM solution was added dropwise to 5.0 mL of an identical substrate solution. Both samples were then left to stir for 30 min at ambient temperature before the solvent was removed *in vacuo*. 1.0 mL of a solution containing 1,3-benzodioxole in CD_3CN was added to dissolve the residue and product yield was determined by ^{1}H NMR against 1,3-benzodioxole. Each measurement was carried out in duplicate. The TON was found to be 2.1 at 8.3 mM and 13.4 at 0.83 mM of **1**.

Ni(0). 0.5 mL of a solution in CH_3CN containing 8.3 mM Ni(dtbbpy)(cod) and 275 mM quinuclidine were prepared and added dropwise to 0.5 mL of a substrate solution containing 250 mM 4′-bromoacetophenone, 375 mM methanol, and 275 mM quinuclidine. Similarly, 5.0 mL of a solution containing 0.83 mM Ni(dtbbpy)(cod) and 275 mM quinuclidine were added dropwise to 5.0 mL of an identical substrate solution. Both samples were then left to stir at ambient temperature for 30 min before the solvent was removed *in vacuo*. 1.0 mL of a solution containing 1,3-benzodioxole in CD_3CN was added to dissolve the residue and product yield was determined by ^{1}H NMR against 1,3-benzodioxole. The TON was found to be 2.0 at 8.3 mM of Ni(0) and 3.9 at 0.83 mM of Ni(0).

K. Oxidative Addition Studies

0.5 mL of a CH_3CN solution containing 12.5 mM Ni(dtbbpy)(cod) and 275 mM quinuclidine was added dropwise to 5.8 mL of one containing 12.5 mM (dtbbpy)NiCl$_2$ and 275 mM quinuclidine. The dark green solution was left to stir for 30 min at ambient temperature before being passed through a 0.22 μm PTFE syringe filter and then added dropwise to a solution of 250 mM 2-bromotoluene. The resulting orange solution was stirred for 20 min and the absorption spectrum was taken with a 2 mm quartz cuvette on a Varian Cary 5000 UV-vis-NIR spectrophotometer (Figure S13A). This was compared to the spectrum of a solution containing 1.0 mM (dtbbpy)Ni(o-tolyl)(Br) in the presence of 250 mM 2-bromotoluene, 275 mM quinuclidine, and 12.5 mM (dtbbpy)NiCl$_2$ (Figure S13B). A similar spectrum is obtained in both cases, suggesting that oxidative addition to the low-valent Ni species generated from **1** forms a Ni(II) aryl species as the terminal product, consistent with a rapid comproportionation reaction between the putative monomeric Ni(I) halide and Ni(III) aryl intermediates.
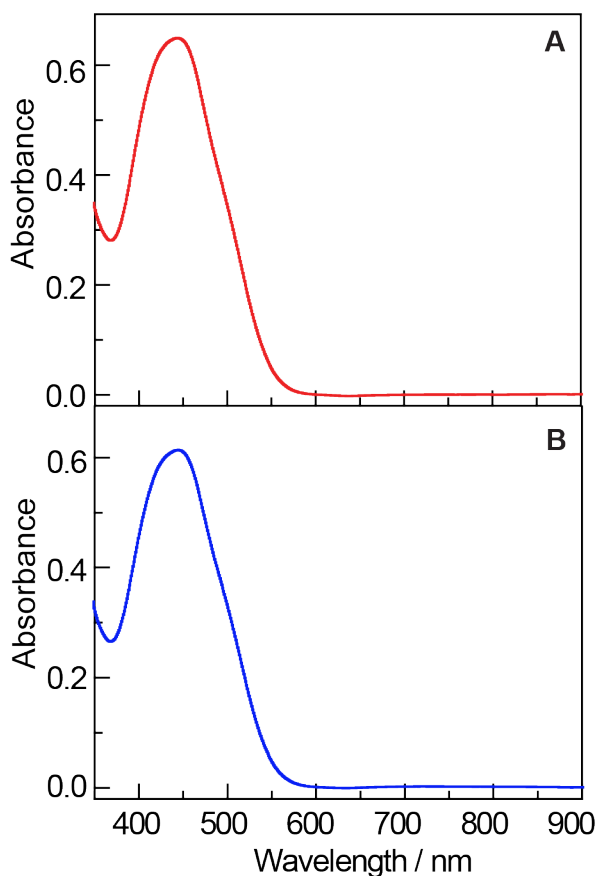
Figure S13 | Spectroscopic studies of oxidative addition. **A** Absorption spectrum of the oxidative addition product. **B** Absorption spectrum of a 1 mM solution of (dtbbpy)Ni(o-tolyl)(Br) under similar conditions. Both spectra are background-corrected for (dtbbpy)NiCl$_2$.

L. Computational Studies

Quinuclidine dimer radical cation. Quantum-mechanical calculations were carried out using density functional theory (DFT) as implemented in Gaussian 16.[8] Geometry optimizations (tight convergence) employed the hybrid functional ωB97XD, which accounts for dispersion and long-range interactions,[9-10] in combination with the polarized triple-zeta basis, def2-TZVP.[11] Solvation effects in CH_3CN were included *via* the conductor-like polarizable continuum model.[12] All optimized structures were verified by frequency calculations, which served to calculate thermodynamic properties at T = 298.15 K. In addition, time-dependent DFT in Gaussian 16 calculated the 30 lowest-energy vertical excitation energies at the same level of theory for the quinuclidine dimer radical cation.
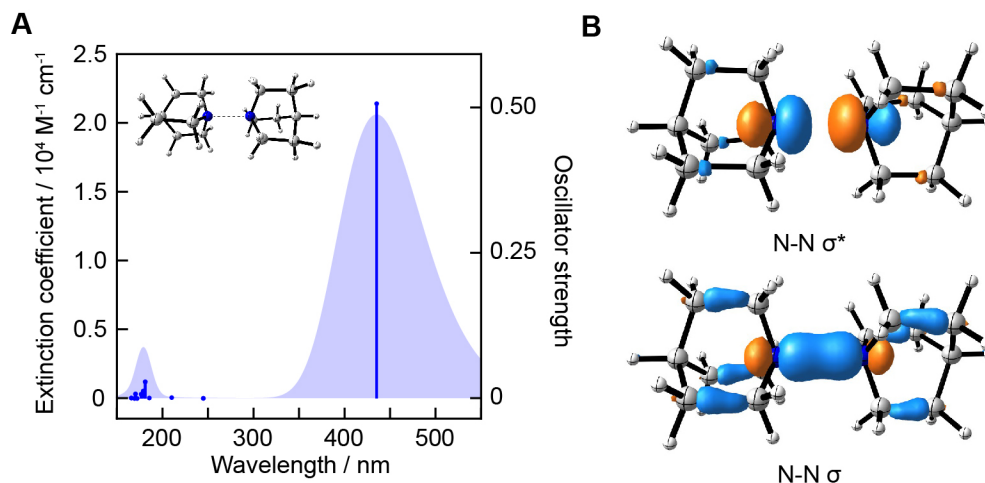
Figure S14 | Computational studies of the quinuclidine dimer radical cation. **A** Simulated absorption line spectrum of the quinuclidine dimer radical cation (blue lines, right y-axis). The line spectrum has been Gaussian-broadened to 0.35 eV at half-width half height to emphasize the high extinction coefficient of the lowest-energy transition at 435 nm (blue shaded, left y-axis). The optimized molecular structure shows a N–N bond length of 2.308 Å and is displayed for reference. We note that the associated absorption line (435 nm) is extremely sensitive to the N–N distance, which is underestimated in our calculations by comparison to the experiment. Marginally increasing the distance to 2.378 Å (frozen bond length geometry optimization) shifts the absorption to 487 nm. **B** Frontier molecular orbitals associated with the lowest-energy transition. The N–N σ orbital involves the p-orbitals of the nitrogen atoms, supported additionally by hyper-conjugation of the parallel C-C σ bonds. The singly-occupied molecular orbital (SOMO, top) features a σ* interaction between the p-orbitals of the same nitrogen atoms.

Energetics of Ni(I/III) comproportionation.
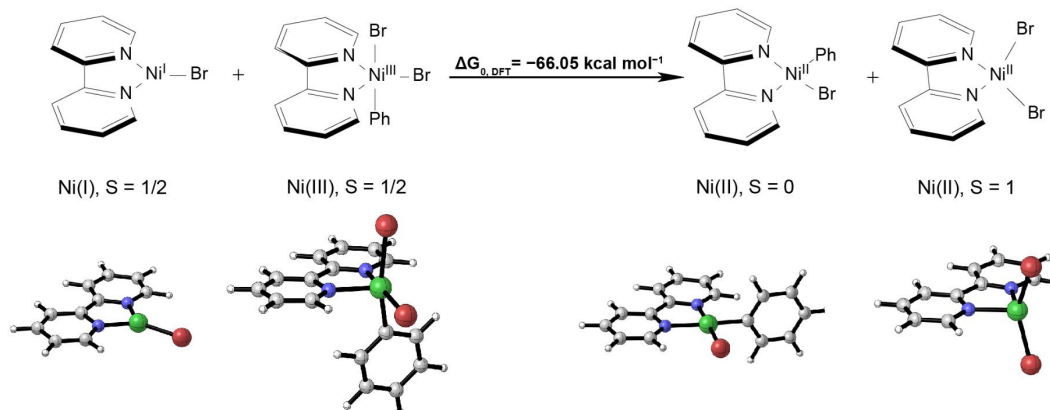
Figure S15 | DFT study demonstrating that comproportionation between a monomeric Ni(I) species and the expected Ni(III) intermediate formed after oxidative addition is highly exergonic.

Complex 1. To additionally support that the crystallographic result for complex **1** is consistent with the intermediate which was spectroscopically observed, we computationally optimized the refined crystal structure in vacuum at the ωB97XD/6-31G* level of theory, whereby we assumed quartet multiplicity as supported by EPR. The optimized molecular structure shows a Ni–Ni bond length of 2.41 Å, slightly underestimating the crystallographic distance of 2.44 Å. Furthermore, the optimized structure differs in the angle between the two bipyridine ligands. This can be quantified by the distance between the *ipso* carbons bearing ^{t}Bu groups on both bipyridine ligands, which is found to be 4.31 Å in the computed structure, in contrast to 4.89 Å in the crystal structure.

Based on the optimized structure, we carried out time-dependent DFT calculations at the same level of theory to compute transitions to the lowest 20 excited states. The corresponding absorption spectrum of the Ni dimer (Figure S16A) shows visible and near-IR transitions, in agreement with the experimentally determined absorption spectrum. The most intense low-energy transition is calculated to be at 732 nm, while the experimentally observed maximum appears at 832 nm (a difference of 1641 cm^{-1}, comparable to the underestimation for the quinuclidine dimer radical cation of 2454 cm^{-1}). This transition is found to result in a metal-to-ligand charge transfer (MLCT) state (Figure S16B), which is likely very sensitive to the Ni–Ni distance. Taking into account that the crystallographic structure displays a longer Ni–Ni bond length, we can tentatively attribute the quantitative difference in the calculated and measured absorption spectrum to an underestimation of the Ni-Ni bond length in our theory. While more theoretical work is required to fully understand the optical properties of complex **1**, our results support the assignment that the observed near-IR absorption features are due to a dimeric Ni compound.
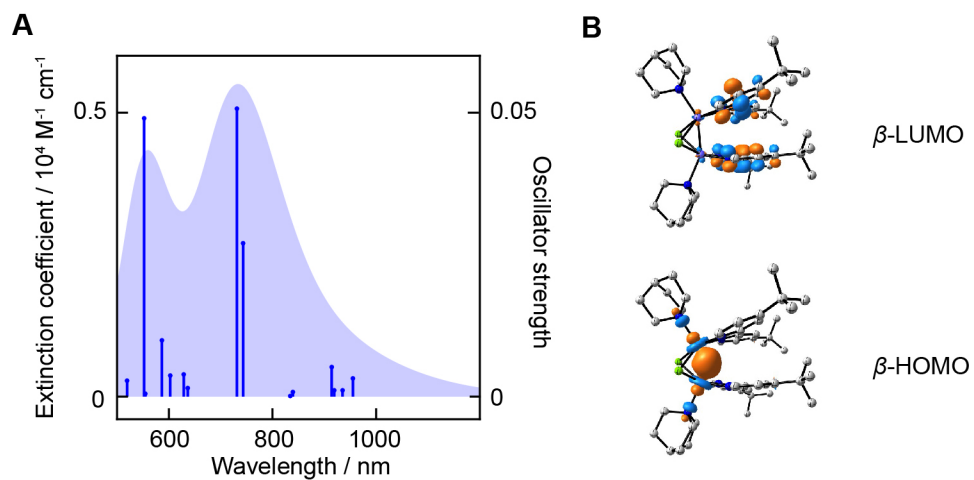
Figure S16 | Computational studies of complex **1**. **A** Simulated absorption line spectrum of **1** (blue lines, right y-axis). The line spectrum has been Gaussian-broadened to 0.2 eV at half-width half height (blue shaded, left y-axis). **B** Frontier molecular orbitals associated with the strongest low-energy transition at 732 nm. The *β*-HOMO (bottom) is characterized predominantly as a σ orbital between the d_{z^2} orbitals of the involved Ni atoms. The *β*-LUMO (top) features π* orbitals of the dtbbpy ligands, classifying the excited state as a MLCT state. Hydrogen atoms are omitted for clarity.

M. Optimized Cartesian Coordinates

	Quinuclidine Dimer Radical Cation		
	x	*y*	*z*
C	0.824828000	3.128288000	–1.178692000
C	–0.000780000	3.655186000	–0.000841000
C	0.900157000	1.581906000	–1.061822000
H	0.358050000	3.414554000	–2.121678000
H	1.829214000	3.551039000	–1.163788000
H	0.601397000	1.092930000	–1.988584000
H	1.905114000	1.248858000	–0.806314000
C	–1.433890000	3.128855000	–0.126386000
H	–2.017161000	3.416079000	0.749080000
H	–1.922806000	3.551275000	–1.004017000
C	–1.371179000	1.582380000	–0.248838000
H	–2.025360000	1.094498000	0.473069000
H	–1.652222000	1.248841000	–1.246695000
H	–0.000830000	4.744490000	–0.001576000
C	0.468193000	1.583597000	1.312208000
H	–0.256205000	1.251855000	2.054770000
H	1.419863000	1.094805000	1.518593000
C	0.606990000	3.129944000	1.303580000
H	0.092232000	3.553782000	2.165602000
H	1.656989000	3.416530000	1.370196000
N	–0.000780000	1.153894000	0.000870000
C	1.433890000	–3.128855000	–0.126386000
C	0.000780000	–3.655186000	–0.000841000
C	1.371179000	–1.582380000	–0.248838000
H	2.017161000	–3.416079000	0.749080000
H	1.922806000	–3.551275000	–1.004017000
H	2.025360000	–1.094498000	0.473069000
H	1.652222000	–1.248841000	–1.246695000
C	–0.606990000	–3.129944000	1.303580000
H	–1.656989000	–3.416530000	1.370196000
H	–0.092232000	–3.553782000	2.165602000
C	–0.468193000	–1.583597000	1.312208000
H	–1.419863000	–1.094805000	1.518593000
H	0.256205000	–1.251855000	2.054770000
H	0.000830000	–4.744490000	–0.001576000
C	–0.900157000	–1.581906000	–1.061822000
H	–1.905114000	–1.248858000	–0.806314000
H	–0.601397000	–1.092930000	–1.988584000
C	–0.824828000	–3.128288000	–1.178692000
H	–1.829214000	–3.551039000	–1.163788000
H	–0.358050000	–3.414554000	–2.121678000
N	0.000780000	–1.153894000	0.000870000

(bpy)Ni^{I}Br			
	x	*y*	*z*
C	–1.388309000	–3.440931000	0.000018000
C	–0.344714000	–2.558747000	0.000058000
C	–1.810206000	–0.702164000	0.000000000
C	–2.915122000	–1.579427000	–0.000055000
C	–2.708110000	–2.927773000	–0.000036000
C	–1.810172000	0.702228000	–0.000001000
C	–0.344594000	2.558742000	–0.000058000
H	0.685779000	2.892822000	–0.000097000
C	–1.388148000	3.440975000	–0.000018000
C	–2.707973000	2.927878000	0.000035000
C	–2.915047000	1.579542000	0.000054000
H	–1.194828000	–4.503129000	0.000038000
H	0.685645000	–2.892872000	0.000097000
H	–3.916526000	–1.171299000	–0.000117000
H	–1.194617000	4.503163000	–0.000038000
H	–3.916469000	1.171460000	0.000116000
N	–0.536736000	1.228530000	–0.000073000
N	–0.536796000	–1.228527000	0.000072000
Ni	0.832247000	–0.000033000	0.000000000
Br	3.147423000	–0.000038000	0.000000000
H	–3.551229000	3.605718000	0.000071000
H	–3.551398000	–3.605574000	–0.000071000

(bpy)Ni^{III}(Ph)Br₂			
	x	y	z
C	−1.504566000	−1.409034000	−3.353362000
C	−0.606754000	−1.348087000	−2.304480000
C	−1.900929000	0.207062000	−1.185530000
C	−2.844578000	0.199812000	−2.199755000
C	−2.639504000	−0.619149000	−3.296858000
C	−2.010519000	1.024546000	0.043522000
C	−1.014704000	1.549475000	2.067004000
H	−0.176117000	1.379605000	2.729182000
C	−2.035233000	2.417118000	2.399420000
C	−3.074900000	2.586858000	1.501311000
C	−3.064829000	1.882778000	0.310794000
H	−1.311329000	−2.062644000	−4.191399000
H	0.300620000	−1.937664000	−2.291116000
H	−3.728291000	0.817043000	−2.142938000
H	−2.007474000	2.945474000	3.340995000
H	−3.869987000	2.004013000	−0.397624000
N	−1.009349000	0.877529000	0.920361000
N	−0.805749000	−0.557710000	−1.255674000
Br	2.374265000	−1.607491000	−0.146060000
Ni	0.407432000	−0.403296000	0.377220000
Br	−0.713894000	−2.207322000	1.676069000
C	1.410105000	1.155645000	−0.200901000
C	1.358936000	1.657984000	−1.485473000
C	2.104628000	1.805949000	0.803019000
C	2.008370000	2.857077000	−1.763403000
H	0.832545000	1.141238000	−2.275558000
C	2.746548000	3.004372000	0.514837000
H	2.160320000	1.396711000	1.805236000
C	2.697847000	3.531663000	−0.767737000
H	1.970392000	3.258373000	−2.768564000
H	3.288173000	3.519289000	1.298445000
H	3.200411000	4.463914000	−0.990844000
H	−3.363922000	−0.639184000	−4.099667000
H	−3.890202000	3.261425000	1.724140000

(bpy)Ni^{II}(Ph)Br		
x	*y*	*z*
Ni 0.149061000	–0.395441000	–0.000030000
N –1.844363000	–0.667305000	0.000037000
C –2.507429000	–1.822133000	0.000073000
H –1.896720000	–2.714266000	0.000080000
C –3.888236000	–1.889440000	0.000101000
H –4.377931000	–2.852556000	0.000129000
N –0.381282000	1.483248000	–0.000039000
C –4.609419000	–0.710217000	0.000093000
C –3.926166000	0.492813000	0.000055000
H –4.472907000	1.423330000	0.000049000
C –2.540975000	0.479740000	0.000026000
C –2.241527000	2.977864000	–0.000043000
H –3.309970000	3.128861000	–0.000025000
C –1.711152000	1.698889000	–0.000020000
C –0.025895000	3.842266000	–0.000110000
H 0.683279000	4.657273000	–0.000148000
C –1.389005000	4.066459000	–0.000089000
C 0.434853000	2.539897000	–0.000084000
H 1.492527000	2.327310000	–0.000099000
C 1.989772000	0.021735000	0.000022000
C 2.684860000	0.226027000	–1.193077000
C 4.014208000	0.633805000	–1.197235000
H 4.527204000	0.789997000	–2.139525000
C 4.685105000	0.842986000	0.000137000
H 5.719829000	1.163094000	0.000180000
C 4.014071000	0.633924000	1.197452000
H 4.526958000	0.790209000	2.139786000
C 2.684722000	0.226149000	1.193180000
H 2.183487000	0.074900000	2.143847000
H –1.788033000	5.071627000	–0.000107000
H –5.690977000	–0.721224000	0.000116000
H 2.183736000	0.074675000	–2.143786000
Br 0.731960000	–2.669059000	–0.000072000

(bpy)Ni^{II}Br$_2$			
	x	y	z
Ni	0.000130000	–0.918330000	0.000000000
Br	–2.274932000	–1.697494000	0.000000000
Br	2.275683000	–1.696095000	0.000000000
N	–0.000227000	0.631629000	1.310835000
C	–0.000234000	0.515913000	2.635163000
C	–0.000369000	1.618139000	3.468013000
H	–0.000370000	1.485392000	4.539945000
C	–0.000493000	2.876770000	2.892804000
H	–0.000592000	3.764176000	3.510980000
C	–0.000493000	2.994206000	1.513648000
H	–0.000593000	3.971237000	1.055030000
C	–0.000361000	1.844028000	0.741247000
N	–0.000227000	0.631629000	–1.310835000
C	–0.000234000	0.515913000	–2.635163000
C	–0.000369000	1.618139000	–3.468013000
H	–0.000370000	1.485392000	–4.539945000
C	–0.000493000	2.876770000	–2.892804000
H	–0.000592000	3.764176000	–3.510980000
C	–0.000493000	2.994206000	–1.513648000
H	–0.000593000	3.971237000	–1.055030000
C	–0.000361000	1.844028000	–0.741247000
H	–0.000126000	–0.492129000	3.028574000
H	–0.000126000	–0.492129000	–3.028574000

	x	y	z
Ni	1.052024000	−1.700886000	0.584003000
Ni	−1.059088000	−1.698958000	−0.582165000
Cl	−0.856084000	−3.009332000	1.465605000
N	−2.521541000	−2.701680000	−1.742965000
N	2.267569000	−0.374118000	−0.380475000
N	2.512484000	−2.704953000	1.746399000
N	−0.659578000	−0.019387000	−1.636289000
C	2.259672000	0.871690000	0.115298000
N	0.658155000	−0.018207000	1.635861000
Cl	0.845949000	−3.014605000	−1.460962000
N	−2.270440000	−0.367016000	0.380091000
C	−1.233277000	1.103831000	−1.160855000
C	−2.257122000	0.878458000	−0.116348000
C	1.236708000	1.102119000	1.159603000
C	0.248621000	0.107248000	−2.608409000
H	0.679538000	−0.822571000	−2.964614000
C	0.663257000	1.333742000	−3.100320000
H	1.423208000	1.348897000	−3.870599000
C	−0.856437000	2.364963000	−1.599174000
H	−1.311749000	3.239836000	−1.150644000
C	−3.158136000	1.853907000	0.305370000
H	−3.135954000	2.830375000	−0.160209000
C	−4.076546000	0.267081000	1.810199000
H	−4.777043000	−0.047056000	2.574125000
C	−3.155598000	−0.651396000	1.341411000
H	−3.103639000	−1.660073000	1.737451000
C	−0.250133000	0.113120000	2.607265000
H	−0.685100000	−0.814587000	2.964078000
C	−0.659918000	1.341795000	3.097833000
H	−1.420275000	1.360760000	3.867625000
C	0.865020000	2.365239000	1.596672000
H	1.324256000	3.237758000	1.147572000
C	3.150926000	−0.662677000	−1.342138000
H	3.094574000	−1.671392000	−1.737522000
C	4.075404000	0.251761000	−1.812003000
H	4.773996000	−0.065609000	−2.576327000
C	3.164711000	1.843006000	−0.307172000
H	3.147146000	2.819684000	0.158167000
C	2.458246000	−4.164055000	1.455506000
H	2.579227000	−4.290115000	0.377667000

H	1.447845000	−4.496858000	1.699165000
C	3.533703000	−4.939625000	2.251386000
H	4.305436000	−5.332482000	1.581277000
H	3.084185000	−5.797254000	2.760283000
C	4.894886000	−2.871894000	2.511591000
H	5.759818000	−3.275097000	1.976579000
H	5.271888000	−2.124160000	3.217229000
C	3.897407000	−2.230825000	1.517334000
H	3.902352000	−1.139731000	1.599352000
H	4.154642000	−2.479738000	0.483876000
C	3.049710000	−3.354862000	4.109277000
H	3.472362000	−2.745295000	4.913902000
H	2.449506000	−4.139869000	4.579813000
C	2.174244000	−2.486915000	3.176164000
H	1.113063000	−2.710421000	3.299449000
H	2.314225000	−1.420139000	3.377654000
C	−0.118913000	2.517757000	2.574749000
C	4.121139000	1.544850000	−1.277976000
C	−4.116389000	1.560199000	1.275669000
C	0.127639000	2.512444000	−2.577881000
C	4.167827000	−3.987358000	3.272142000
H	4.867715000	−4.526554000	3.915645000
C	−4.179869000	−3.982516000	−3.266745000
H	−4.881022000	−4.521028000	−3.909444000
C	−3.548594000	−4.934554000	−2.244012000
H	−3.101259000	−5.794375000	−2.751129000
H	−4.321574000	−5.324034000	−1.573368000
C	−2.471248000	−4.160379000	−1.449320000
H	−2.592799000	−4.284099000	−0.371273000
H	−1.461688000	−4.496306000	−1.692145000
C	−3.059842000	−3.354585000	−4.104758000
H	−3.480636000	−2.745455000	−4.910684000
H	−2.461597000	−4.142100000	−4.573597000
C	−4.904180000	−2.863721000	−2.508458000
H	−5.770255000	−3.263715000	−1.972882000
H	−5.279115000	−2.116328000	−3.215550000
C	−3.905243000	−2.223412000	−1.515173000
H	−3.907186000	−1.132458000	−1.599254000
H	−4.163435000	−2.469634000	−0.481310000
C	−2.182357000	−2.487187000	−3.173048000
H	−1.121738000	−2.713702000	−3.295642000
H	−2.319527000	−1.420426000	−3.376556000
C	−0.545183000	3.913935000	3.025636000

C	–0.913441000	4.756447000	1.789811000
H	–0.050103000	4.932580000	1.142442000
H	–1.689996000	4.260258000	1.198627000
H	–1.292752000	5.734137000	2.101091000
C	0.630322000	4.576383000	3.768723000
H	0.348845000	5.581748000	4.096327000
H	0.912339000	3.996150000	4.652012000
H	1.511966000	4.666777000	3.126956000
C	–1.761335000	3.858609000	3.957188000
H	–2.603183000	3.352728000	3.474368000
H	–1.537181000	3.340977000	4.894636000
H	–2.079683000	4.872955000	4.212281000
C	5.232472000	2.521800000	–1.667979000
C	6.491303000	2.110359000	–0.875363000
H	7.322725000	2.778380000	–1.120035000
H	6.313119000	2.166890000	0.202820000
H	6.794941000	1.087432000	–1.116715000
C	4.878171000	3.974491000	–1.317490000
H	3.959607000	4.300629000	–1.814881000
H	4.764922000	4.125981000	–0.239792000
H	5.685301000	4.634251000	–1.646466000
C	5.539323000	2.443510000	–3.174129000
H	5.933021000	1.467694000	–3.469258000
H	4.652970000	2.651464000	–3.780485000
H	6.301450000	3.184680000	–3.429792000
C	–5.223704000	2.541989000	1.664926000
C	–5.529347000	2.467475000	3.171529000
H	–5.926049000	1.493541000	3.468833000
H	–4.641677000	2.673475000	3.776609000
H	–6.288679000	3.211710000	3.426617000
C	–4.864392000	3.992722000	1.311523000
H	–3.944266000	4.316448000	1.807630000
H	–4.751433000	4.141799000	0.233452000
H	–5.668860000	4.656008000	1.639931000
C	–6.484833000	2.133863000	0.874246000
H	–6.307382000	2.187653000	–0.204195000
H	–6.792195000	1.112579000	1.117821000
H	–7.313461000	2.805538000	1.118390000
C	0.559620000	3.906345000	–3.030346000
C	1.775563000	3.844900000	–3.961798000
H	2.615145000	3.335701000	–3.478501000
H	1.549190000	3.327496000	–4.898838000
H	2.098384000	4.857625000	–4.217735000

C	0.931314000	4.748895000	−1.795605000
H	0.068826000	4.928982000	−1.148201000
H	1.706191000	4.250511000	−1.204087000
H	1.314137000	5.724813000	−2.108143000
C	−0.613214000	4.572633000	−3.774244000

N. X-ray Crystallography

A CH_3CN solution was prepared by the dropwise addition of 5 mL of a 5 mM solution of Ni(dtbbpy)(cod) to $NiCl_2$(dme) (30.9 mg), dtbbpy (37.7 mg), and quinuclidine (153 mg) in 5 mL CH_3CN. This solution was then washed with 5 × 5 mL pentane and quinuclidine (153 mg) was added to the CH_3CN fraction, from which crystals of **1** were grown at –25 °C. X-ray diffraction data were collected on a Bruker three-circle platform goniometer equipped with an Apex II CCD detector and Oxford Cryosystems Cryostat cooling device using φ and ω scans. A fine-focus sealed tube Mo Kα (0.71073 Å) X-ray source was used. The crystal was mounted on a cryoloop using Paratone oil. Data were integrated using SAINT and multi-scan absorption correction was applied using SADABS. The structure was solved by intrinsic phasing using SHELXT (APEX3 program suite, 2016) and refined against F^2 on all data by full matrix least squares with SHELXL. All non-hydrogen atoms, including the disorder fragments, were located in the difference-Fourier maps and refined anisotropically. Hydrogen atoms were added at calculated positions and refined with a riding model. The restraints on bond lengths (SADI/SAME) and atomic displacement parameters (SIMU/RIGU) have been applied on each pair of disorder fragments as necessary. The structure was modelled as a two-part inversion twin. Two units of **1** are included in the crystallographic asymmetric unit.

Table S3. Crystal data and structure refinement for **1**.

Empirical formula	$C_{114}H_{169}Cl_6N_{19}Ni_4$
Formula weight	2253.17
T (K)	100(2)
λ (Å)	0.71073
Crystal system	Orthorhombic
Space group	$Pca2_1$
a (Å)	28.293(3)
b (Å)	12.7260(16)
c (Å)	33.847(4)
α (°)	90
β (°)	90
γ (°)	90
V (Å^3)	12187(2)
Z	4
ρ_{calcd} (Mg/m^3)	0.307
μ (mm^{-1})	0.792
θ range for data collection (°)	2.31 to 25.02
Index ranges	$-33 \le h \le 33, -15 \le k \le 15, -40 \le \ell \le 39$
Reflections collected	99146
Independent reflns (R_{int})	21501 (0.0702)
Completeness to θ_{max}	99.6%
Data/restraints/parameters	21501 / 1851 / 1743
GOF on F^2	1.095
R1	0.0600
wR2	0.1421
Largest diff. peak, hole (e Å^{-3})	0.519, –0.531

Table S4. Selected bond distances and angles for compound **1**.

Atom Label	Bond Distances (Å)
Ni(1)–Ni(2)	2.4427(17)
Ni(1)–Cl(1)	2.411(3)
Ni(1)–Cl(2)	2.404(2)
Ni(1)–N(1)	2.014(7)
Ni(1)–N(2)	2.025(7)
Ni(1)–N(6)	2.167(8)
Ni(2)–Cl(1)	2.415(3)
Ni(2)–Cl(2)	2.400(2)
Ni(2)–N(3)	2.026(7)
Ni(2)–N(4)	2.039(7)
Ni(2)–N(5)	2.127(8)

Atom Label	Bond Angles (°)
Ni(1)–Cl(1)–Ni(2)	60.81(7)
Ni(1)–Cl(2)–Ni(2)	61.12(6)
Cl(1)–Ni(1)–Cl(2)	84.23(8)
N(1)–Ni(1)–Cl(1)	95.4(2)
N(1)–Ni(1)–Cl(2)	162.5(2)
N(1)–Ni(1)–N(2)	79.7(3)
N(1)–Ni(1)–N(6)	97.2(3)
N(6)–Ni(1)–Ni(2)	150.0(2)
Cl(1)–Ni(2)–Cl(2)	84.25(9)
N(3)–Ni(2)–Cl(1)	93.9(2)
N(3)–Ni(2)–Cl(2)	158.5(2)
N(3)–Ni(2)–N(4)	79.9(3)
N(3)–Ni(2)–N(5)	102.9(3)
N(5)–Ni(2)–Ni(1)	149.5(2)

O. References

1. Pangborn, A. B.; Giardello, M. A.; Grubbs, R. H.; Rosen, R. K.; Timmers, F. J., Safe and Convenient Procedure for Solvent Purification. *Organometallics* **1996**, *15*, 1518–1520.

2. Terrett, J. A.; Cuthbertson, J. D.; Shurtleff, V. W.; MacMillan, D. W. C., Switching on Elusive Organometallic Mechanisms with Photoredox Catalysis. *Nature* **2015**, *524*, 330–334.

3. Shields, B. J.; Kudisch, B.; Scholes, G. D.; Doyle, A. G., Long-Lived Charge-Transfer States of Nickel(II) Aryl Halide Complexes Facilitate Bimolecular Photoinduced Electron Transfer. *J. Am. Chem. Soc.* **2018**, *140*, 3035–3039.

4. Shields, B. J.; Doyle, A. G., Direct C(sp^3)–H Cross Coupling Enabled by Catalytic Generation of Chlorine Radicals. *J. Am. Chem. Soc.* **2016**, *138*, 12719–12722.

5. Hatchard, C. G.; Parker, C. A.; Bowen, J. B., A New Sensitive Chemical Actinometer - II. Potassium Ferrioxalate as a Standard Chemical Actinometer. *Proc. Royal Soc. London Ser. A. Math. and Phys. Sci.* **1956**, *235*, 518–536.

6. Holder, P. G.; Pizano, A. A.; Anderson, B. L.; Stubbe, J.; Nocera, D. G., Deciphering Radical Transport in the Large Subunit of Class I Ribonucleotide Reductase. *J. Am. Chem. Soc.* **2012**, *134*, 1172–1180.

7. Halpern, A. M.; Forsyth, D. A.; Nosowitz, M., Flash Photolysis of Saturated Amines in Acetonitrile Solution at 248 nm: Formation of Radical Cations. *J. Phys. Chem.* **1986**, *90*, 2677–2679.

8. Frisch, M. J.; Trucks, G. W.; Schlegel, H. B.; Scuseria, G. E.; Robb, M. A.; Cheeseman, J. R.; Scalmani, G.; Barone, V.; Petersson, G. A.; Nakatsuji, H.; Li, X.; Caricato, M.; Marenich, A. V.; Bloino, J.; Janesko, B. G.; Gomperts, R.; Mennucci, B.; Hratchian, H. P.; Ortiz, J. V.; Izmaylov, A. F.; Sonnenberg, J. L.; Williams; Ding, F.; Lipparini, F.; Egidi, F.; Goings, J.; Peng, B.; Petrone, A.; Henderson, T.; Ranasinghe, D.; Zakrzewski, V. G.; Gao, J.; Rega, N.; Zheng, G.; Liang, W.; Hada, M.; Ehara, M.; Toyota, K.; Fukuda, R.; Hasegawa, J.; Ishida, M.; Nakajima, T.; Honda, Y.; Kitao, O.; Nakai, H.; Vreven, T.; Throssell, K.; Montgomery Jr., J. A.; Peralta, J. E.; Ogliaro, F.; Bearpark, M. J.; Heyd, J. J.; Brothers, E. N.; Kudin, K. N.; Staroverov, V. N.; Keith, T. A.; Kobayashi, R.; Normand, J.; Raghavachari, K.; Rendell, A. P.; Burant, J. C.; Iyengar, S. S.; Tomasi, J.; Cossi, M.; Millam, J. M.; Klene, M.; Adamo, C.; Cammi, R.; Ochterski, J. W.; Martin, R. L.; Morokuma, K.; Farkas, O.; Foresman, J. B.; Fox, D. J. *Gaussian 16 Rev. B.01*, Wallingford, CT, 2016.

9. Chai, J.-D.; Head-Gordon, M., Long-Range Corrected Hybrid Density Functionals with Damped Atom–Atom Dispersion Corrections. *Phys. Chem. Chem. Phys.* **2008**, *10*, 6615–6620.

10. Minenkov, Y.; Singstad, Å.; Occhipinti, G.; Jensen, V. R., The Accuracy of DFT-Optimized Geometries of Functional Transition Metal Compounds: A Validation Study of Catalysts for Olefin Metathesis and Other Reactions in the Homogeneous Phase. *Dalton Trans.* **2012**, *41*, 5526–5541.

11. Weigend, F.; Ahlrichs, R., Balanced Basis Sets of Split Valence, Triple Zeta Valence and Quadruple Zeta Valence Quality for H to Rn: Design and Assessment of Accuracy. *Phys. Chem. Chem. Phys.* **2005**, *7*, 3297–3305.

12. Barone, V.; Cossi, M., Quantum Calculation of Molecular Energies and Energy Gradients in Solution by a Conductor Solvent Model. *J. Phys. Chem. A* **1998,** *102*, 1995–2001.